Electronic-state interference in the C 1*s* excitation and decay of methyl chloride studied by angularly resolved Auger spectroscopy

S. Nandi,[1,*] C. Nicolas,[1] A. N. Artemyev,[2] N. M. Novikovskiy,[3] C. Miron,[1,4,5] J. D. Bozek,[1] and Ph. V. Demekhin[2,3,†]

[1]*Synchrotron SOLEIL, L'Orme des Merisiers, Saint-Aubin, BP 48, 91192 Gif-sur-Yvette Cedex, France*

[2]*Institut für Physik und CINSaT, Universität Kassel, Heinrich-Plett-Straße 40, 34132 Kassel, Germany*

[3]*Research Institute of Physics, Southern Federal University, Stachki Avenue 194, 344090 Rostov-on-Don, Russia*

[4]*Extreme Light Infrastructure–Nuclear Physics, Horia Hulubei National Institute for Physics and Nuclear Engineering, 30 Reactorului Street, 077125 Măgurele, Judetul Ilfov, Romania*

[5]*LIDYL, CEA, CNRS, Université Paris-Saclay, CEA Saclay, 91191 Gif-sur-Yvette, France*

(Received 12 August 2017; published 3 November 2017)

Resonant Auger (RA) decay spectra of carbon 1*s* excited CH_3Cl molecules are recorded with angular resolution using linearly polarized synchrotron radiation. The selected photon energies corresponding to the C $1s \rightarrow 8a_1$ core to lowest unoccupied molecular orbital and C $1s \rightarrow 4sa_1$, $4pe$, and $4pa_1$ core to Rydberg excitations of methyl chloride are used and electrons in the binding energy range of 11–37 eV are detected. The vibrationally unresolved RA electron angular distributions, recorded for participator Auger transitions populating the X, A, B, and C states of the CH_3Cl^+ ion, exhibit strong variations across the selected electronic resonances. These observations are interpreted with the help of *ab initio* electronic structure and dynamics calculations, which account for electronic-state interference between the direct and different resonant ionization pathways. For spectator transitions, the theory predicts almost isotropic angular distributions with moderate changes of β parameters around zero, which is in agreement with the experimental observations.

DOI: 10.1103/PhysRevA.96.052501

I. INTRODUCTION

Interference between the amplitudes for coherent excitation and decay of intermediate electronic resonances overlapping within their natural lifetime widths is usually referred to as electronic-state interference (ESI) [1]. If close-lying resonances have equal symmetry and can thus decay into the same final continuum state, the total photoionization probability is given by the square of the coherent superposition of the corresponding amplitudes for ionization pathways involving different intermediate resonances. This is an atomic analog of the double-slit experiment [2]. Electronic-state interference has previously been identified in the angularly unresolved resonant Auger (RA) electron spectra of core-excited atoms [3–10] and molecules [11].

Angularly resolved decay spectra are more sensitive to such interference effects [12,13]. This sensitivity has been utilized to reveal ESI and lifetime vibrational interference [14] (LVI) in the angularly resolved RA decay and fluorescence emission spectra of atoms [15–19], diatomic molecules [20–27], and even polyatomic [28–33] molecules. These studies have shown that ESI between the weak direct and dominant resonant ionization pathways induces long-range energy dispersions of the angular emission distribution parameters across the resonances. In addition, ESI and LVI become significantly more pronounced in angularly resolved spectra, even for well-separated resonances that exhibit very weak effects in the angularly averaged spectra. Finally, ESI between electronic resonances with different symmetries, which is strictly forbidden in the total spectra, can be observed in angularly resolved emission spectra [22,25,26].

In the present work we use the high sensitivity of angularly resolved electron spectroscopy [13] to investigate ESI in the CH_3Cl molecule. The dynamics of the core excitation and decay of methyl chloride at its C 1*s*, Cl 1*s*, and Cl 2*p* edges has been previously studied by electron-impact energy-loss spectroscopy [34,35], photoion yield spectroscopy [36], Auger electron spectroscopy [11,37], Auger electron-ion coincidence spectroscopy [38], and resonant inelastic x-ray scattering [37,39], all without angular resolution. At the Cl K edge, sizable ESI effects were identified in the partial Auger electron spectra [11]. The C 1*s* excitation spectrum of methyl chloride exhibits many overlapping pre-edge resonances [34–36], offering a rich opportunity to study ESI. In this work we concentrate on the carbon K edge of methyl chloride and investigate angular emission distributions of RA electrons.

The paper is organized as follows. Experimental and theoretical methods are outlined in Secs. II and III, respectively. The RA electron angular distributions measured and computed for different participator and spectator decay channels are discussed in Sec. IV. We conclude in Sec. V with a brief summary.

II. EXPERIMENT

The experiment was carried out at the French national synchrotron radiation facility SOLEIL, using the PLEIADES beamline, which allows for high-resolution soft-x-ray studies of gaseous atoms [40], molecules [41], clusters [42], nanoparticles [43], and large biologically relevant species [44]. A variable groove depth, 600-lines/mm plane grating was used to monochromatize the radiation from an Apple II–type permanent magnet undulator. The width of the exit slit of the monochromator was set to 7 μm, which resulted in a photon bandwidth of about 23 meV. Commercially available, high-purity (99.95%) methyl chloride gas from Air Liquide

*Present address: Department of Physics, Lund University, PO Box 118, 221 00 Lund, Sweden.

†demekhin@physik.uni-kassel.de

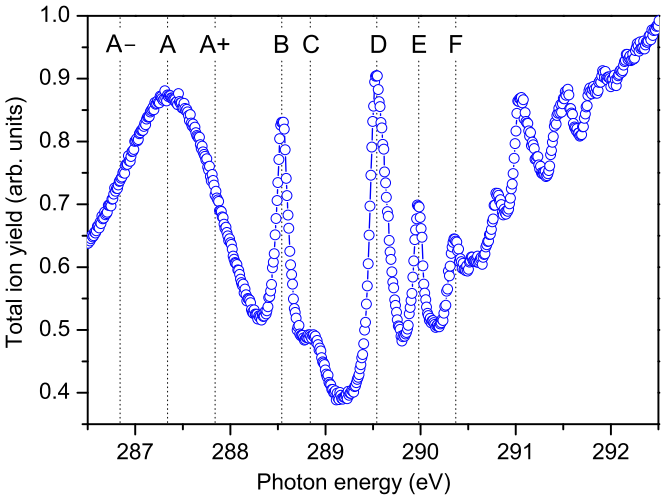

FIG. 1. Total ion yield of methyl chloride recorded in the vicinity of the K edge of the carbon atom. The vertical dotted lines indicate photon energies selected to measure the angularly resolved RA electron spectra in Figs. 2 and 3. Assignment and energy positions of the resonant features, labeled by capital letters A–F at the top, are listed in Table I. The two photon energies detuned from the transition energy of the resonance A by ±0.5 eV are labeled as A±.

was used as the target. The total ion yield was recorded near the carbon K edge as a function of the photon energy with steps of 10 meV. For this measurement, the target gas was introduced inside a yield chamber as an effusive jet of molecules. The pressure inside the chamber was kept close to 5×10^{-6} mbar to ensure adequate count rate.

The total ion yield of methyl chloride, recorded in the vicinity of the carbon 1s ionization threshold, is depicted in Fig. 1. This yield exhibits prominent features owing to the resonant excitation of the 1s core electron of carbon atom into different unoccupied orbitals. Several resonant transitions, relevant for the present study, are marked by capital letters at the top of the figure. Their energy positions and assignments according to Refs. [34–36] are listed in Table I. The electronic configuration of methyl chloride in its neutral ground state can be written as

$$\left[1s_{\mathrm{Cl}}^2 1s_{\mathrm{C}}^2 2s_{\mathrm{Cl}}^2 2p_{\mathrm{Cl}}^6\right] 5a_1^2 6a_1^2 2e^4 7a_1^2 3e^4.$$

TABLE I. Energy positions of selected resonant features in the total absorption spectrum in Fig. 1 and their assignment according to Refs. [34–36]. The present photon energy was calibrated according to Ref. [36].

	Energy (eV)		Assignment
Label	Present work	Ref. [36]	Refs. [34–36]
A	287.34	287.34	$8a_1(\upsilon_{\text{C-Cl}})$
B	288.54	288.45	$4sa_1$
C	288.84	288.79	$4sa_1(\upsilon_{\text{CH}})$
D	289.54	289.50	$4pe$
E	289.98	289.95	$4pe(\upsilon_{\text{CH}})$
F	290.37	290.37	$4pa_1$

In this notation, the carbon and chlorine core electrons are uniquely indicated in square brackets and the valence electrons are given by the irreducible representations of the C_{3v} group.

The first intense resonant feature in Fig. 1, labeled as A, corresponds to the excitation of the C 1s electron to the lowest unoccupied molecular orbital $8a_1$, which has an antibonding character. The resulting core-excited state dissociates along the C-Cl coordinate and the respective resonant signal is accordingly broadened [34–36]. The sharper features at higher photon energies, labeled B–F, correspond to the excitation of $4sa_1$, $4pe$, and $4pa_1$ Rydberg states, together with their CH symmetric stretching vibrational mode [34–36] (see the last column of Table I). The photon energy was calibrated with respect to the C $1s \rightarrow 8a_1$ as well as $1s \rightarrow 4pa_1$ transition energies from Ref. [36] (resonances A and F in Table I).

The RA electron spectra were recorded at the photon energies of the resonances A–F as indicated by the vertical dotted lines in Fig. 1. Two additional measurements were performed at photon energies 286.84 and 287.84 eV, detuned from the transition energy of the resonance A maximum by ±0.5 eV (labeled throughout as A±). The spectra were recorded using a VG Scienta R4000 hemispherical electron spectrometer. During the spectra acquisition, the target gas was introduced inside a differentially pumped gas cell, containing five electrodes used to compensate the plasma potential gradient along the photon beam, ensuring thereby the highest possible spectrometer resolution. The pressure inside the spectrometer chamber was maintained at around 1×10^{-5} mbar, with that inside the gas cell being typically two orders of magnitude higher.

A curved entrance slit of 0.3 mm was used in the spectrometer with a pass energy of 50 eV for the electrons. Combining these factors, the total experimental broadening was around 44 meV for all measured spectra. In addition, the translational Doppler broadening due to the random thermal motion of the target molecules was estimated to be between 25 and 28 meV for the electron kinetic energies measured. The spectra were recorded at 0° and 90° with respect to the polarization axis of the incident photon beam. The spectra I_0 and I_{90} measured at the two angles were carefully normalized with respect to the average photon flux, the individual collection time, and the corresponding spectrometer chamber pressure, to enable an accurate determination of the angular asymmetry parameters.

Figure 2 shows the electron spectra as functions of the binding energy determined at the magic angle (54.7° with respect to the polarization of the incident photons) via the well-known relation $I = (I_0 + 2I_{90})/3$. As one can see, vibronic band structures, present in these spectra, possess strong variations with respect to the excitation energy (increasing from top to bottom; see the assignment at the left-hand side of each spectrum). The corresponding angular distribution parameters, extracted for each excitation energy via the $\beta = 2(I_0 - I_{90})/(I_0 + 2I_{90})$ relation, are depicted in Fig. 3 as functions of the binding energy. One can see that these β parameters vary strongly as functions of the binding energy: from large positive values at lower binding energies to small values of different sign for larger binding energies. These variations with respect to the binding energy are also very different for different excitation energies.

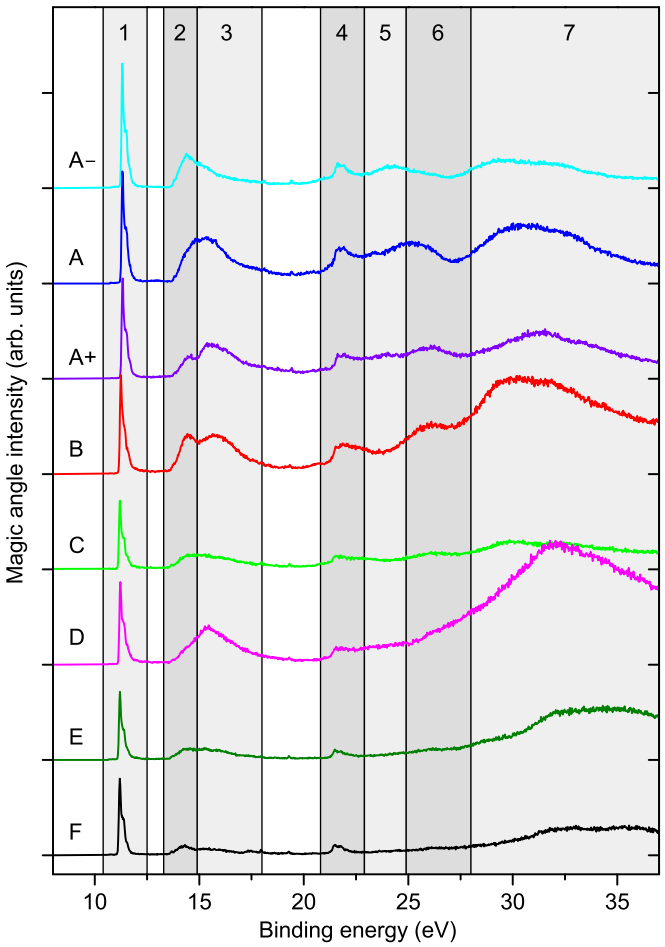

FIG. 2. Magic angle RA electron spectra of methyl chloride as functions of the binding energy. The spectra were measured at different excitation energies, as indicated by the capital letters at the left-hand-side vertical axis (see Table I for the photon energy and assignment). The gray-shaded areas indicate seven binding energy intervals used to determine integral angular distribution parameters. Their assignment as enumerated at the top of the figure is given in Table II.

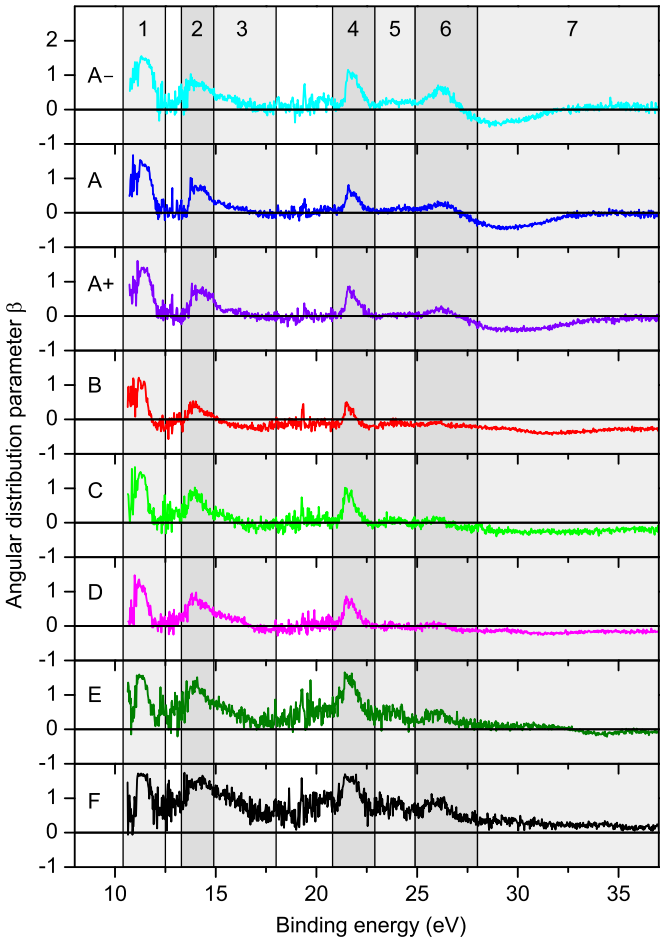

FIG. 3. Angular distribution parameters of RA electrons as functions of the binding energy. Each panel corresponds to different excitation energy, as indicated by capital letters at the left-hand-side (see the notation in Fig. 2).

III. THEORY

In order to interpret the experimental RA electron spectra of methyl chloride, we applied the theoretical approach that was previously used to investigate angular resolved core ionization and core excitation spectra of diatomic [23–26], polyatomic [31–33], and chiral [45,46] molecules. In the vicinity of core excitation, the total transition amplitude is given by the coherent superposition of the amplitudes for the direct and different resonant (i.e., excitation and decay of the intermediate state) ionization pathways:

$$D_k(\Lambda_0\chi_0,\Lambda_i\chi_i\varepsilon\ell m) = \langle\Lambda_i\chi_i\varepsilon\ell m|\mathbf{d}_k|\Lambda_0\chi_0\rangle + \sum_{\Lambda_r\chi_r}\frac{\langle\Lambda_i\chi_i\varepsilon\ell m|\mathbf{H^{ee}}|\Lambda_r\chi_r\rangle\langle\Lambda_r\chi_r|\mathbf{d}_k|\Lambda_0\chi_0\rangle}{\omega - E_{\Lambda_r\chi_r} + i\Gamma_{\Lambda_r\chi_r}/2}. \quad (1)$$

In this equation, $\mathbf{H^{ee}}$ is the operator for the electrostatic Coulomb interaction and $\mathbf{d}_k$ is the electric dipole transition operator for the absorption of a photon with polarization k defined in the molecular frame. Indices Λ_0, Λ_r, and Λ_i designate initial ground, intermediate excited, and final ionic electronic states of a molecule; χ stands for the wave function for the nuclear motion; and quantum numbers $\varepsilon\ell m$ describe a photoelectron partial wave with the kinetic energy ε, orbital angular momentum ℓ, and its projection m on the molecular quantization axis. The energy positions of vibronic resonances and their Auger decay widths are denoted by $E_{\Lambda_r\chi_r}$ and $\Gamma_{\Lambda_r\chi_r}$, respectively, whereas photon energy ω is related to the photoelectron energy and ionization potential via $\omega = V_I + \varepsilon$.

The electronic transition amplitudes for the ionization, excitation, and decay were computed by the single-center method and code [47–49]. It provides an accurate description of the partial continuum photoelectron waves in the field of the molecular potential, which includes interaction of a photoelectron with all nuclei and electrons in the occupied orbitals of the ion. Molecular orbitals of the core-excited Rydberg electrons $4sa_1$, $4pe$, and $4pa_1$ were computed as described in detail in our previous works [50–53]. The electronic transition amplitudes were computed at the equilibrium internuclear geometry of the ground electronic state of CH_3Cl in the relaxed-core Hartree-Fock approximation including monopole

relaxation of the molecular orbitals in the field of the core vacancy [23–26,31–33].

The working equations required to compute vibrationally and angularly resolved RA electron spectra of polyatomic molecules are reported in Ref. [31] [see Eqs. (7)–(10) therein]. These equations relate the total photoionization cross sections $\sigma_{\Lambda_i\chi_i}(\omega)$ for the population of a particular final vibronic $\Lambda_i\chi_i$ state of a molecular ion and the respective angular distribution parameters $\beta_{\Lambda_i\chi_i}(\omega)$ with the partial transition amplitudes (1). In the present work (see Sec. IV), the experimental angularly resolved RA electron spectra are analyzed for the whole vibrational band of a particular electronic transition, i.e., in the vibrationally unresolved mode. In order to enable comparison with the experiment, the computed vibrationally resolved spectra should be averaged over all vibrational states χ_i of the ion.

However, there is a more elegant way to access vibrationally unresolved angular distribution parameters, which was introduced and tested in our previous work [31]. As explicitly demonstrated in the Appendix of this reference, summation over the final vibrational state can be performed analytically. This approach also significantly reduces the computational efforts, since only Franck-Condon factors for the resonant excitation (i.e., the shape of the excitation profile in the total absorption) are required to compute vibrationally unresolved spectra. Importantly, such a summation does not eliminate ESI effects [sum of the first and second terms in Eq. (1) together with the summation over index Λ_r in the second term]. However, integration over χ_i eliminates LVI effects [sum over index χ_r in the second term of Eq. (1)].

The required Franck-Condon factors for resonant excitation were computed in the present work by the one-dimensional nuclear dynamics simulations. In the calculations, we considered main dynamical modes, which were assigned in Refs. [34–36] to the resonant features in the excitation spectrum (see Table I). In particular, for the $8a_1$ electronic state, only the dissociative motion along the C-Cl coordinate was taken into account. For the 4ℓ Rydberg electronic states, only the symmetric CH stretching vibrational mode was accounted for. The one-dimensional cuts of the respective potential energy surfaces along the chosen coordinates were computed by the coupled-cluster theory with single, double, and partially triple excitation [CCSD(T)] or renormalized R-CCSD(T) methods [54] with the cc-pvtz basis set using the MOLPRO quantum chemistry suite [55]. Potential energy curves of the excited states were computed within the equivalent core $Z+1$ approximation.

In this approximation, the carbon core-excited $8a_1$ state of the CH_3Cl molecule is equivalent to the neutral ground state of the NH_3Cl molecule. Furthermore, we assumed that the potential energy curves of the core-excited 4ℓ Rydberg states do not differ much from that of the core-ionized state, i.e., the delocalized Rydberg electron influences the shape of the ionic energy curve only slightly. We therefore computed energy curves for the ground state of the NH_3Cl^+ molecular ion. The computed excitation profile for the dissociative $8a_1$ core-excited state is very similar to the lowermost broad feature in Fig. 1. Finally, the computed energy splitting between the vibrational states of the CH symmetric stretching mode of the carbon core-ionized state is equal to 0.4 eV, whereas the excitation probabilities for the first three vibrational states are related as 0.58:0.35:0.07.

TABLE II. Binding energy intervals used to determine integral angular distribution parameters, as visualized by gray-shaded areas and enumerated at the top of Figs. 2 and 3. The type of the RA decay transition and corresponding final ionic states, encompassed in each interval, are indicated in the last two columns. Symbols P and S stand for participator and spectator transitions, whereas R in the assignments of spectator final states designates the excited resonance.

No.	Interval (eV)	Transition	Final state
1	10.4–12.5	P	$3e^{-1}$
2	13.3–14.9	P	$7a_1^{-1}$
3	14.9–18.0	P	$2e^{-1}$
4	20.8–22.9	P + S	$6a_1^{-1} + 3e^{-2}R$
5	22.9–24.9	P + S	$5a_1^{-1} + 7a_1^{-1}3e^{-1}R$
6	24.9–28.0	P + S	$+2e^{-1}3e^{-1}R + 7a_1^{-2}R$
7	28.0–37.0	P + S	$+2e^{-1}7a_1^{-1}R + 2e^{-2}R$

IV. RESULTS AND DISCUSSION

This section is organized as follows. In Sec. IV A we analyze experimental RA electron spectra and report vibrationally unresolved angular distribution parameters. The measured and computed angular distribution parameters for the participator and spectator transitions are compared and further analyzed in Secs. IV B and IV C, respectively.

A. Analysis of the experimental data

It is difficult to resolve individual vibronic states within the strongly overlapping band structures of each final electronic states as shown in Fig. 2. Moreover, for higher binding energies (see below), it is not even possible to separate contributions from different final electronic states. Therefore, in order to analyze the experimental angularly resolved RA electron spectra, we will use the strategy introduced by different authors to study angularly resolved photoionization of valence orbitals of methyl chloride [56]. Based on the *ab initio* electronic structure calculations, it was suggested in this reference to divide the binding energy range into several intervals, which encompass different individual or several overlapping electronic states of the ion. The binding energy intervals used here and their assignments are specified in Table II and highlighted by gray-shaded areas in Figs. 2 and 3.

The first three intervals encompass individual electronic states of the ion representing ionization of the $3e$, $7a_1$, and $2e$ outermost valence molecular orbitals as seen from the lower panel of Fig. 1 in Ref. [56]. The $3e^{-1}(X\,^2E)$, $7a_1^{-1}(A\,^2A_1)$, and $2e^{-1}(B\,^2E)$ ionic states are of one-hole character and are populated by the RA decay via participator transitions. The fourth binding energy interval encompasses the $6a_1^{-1}(C\,^2A_1)$ one-hole ionic state [56], which is produced by participator RA decay as well. In Sec. IV C we will show that the lowermost in energy $3e^{-2}R$ two-hole–one-particle electronic states, populated by spectator RA decay, contribute to the fourth binding energy interval as well. These satellite states could not be identified in Ref. [56], since they have very

TABLE III. Integral angular distribution parameters β recorded in the present work at different excitation energies in the vicinity of the carbon K edge of methyl chloride (as assigned in Table I) and determined for different binding energy intervals (as enumerated in Table II). The experimental statistical uncertainties are given in parentheses as $1.404(4) \equiv 1.404 \pm 0.004$.

Label	Interval 1	Interval 2	Interval 3	Interval 4	Interval 5	Interval 6	Interval 7
A–	1.404(4)	0.656(5)	0.238(4)	0.570(5)	0.203(4)	0.220(4)	−0.137(2)
A	1.294(4)	0.567(5)	0.140(3)	0.308(3)	0.089(3)	0.093(2)	−0.216(1)
A+	1.249(5)	0.619(6)	0.104(3)	0.312(4)	0.027(3)	0.049(3)	−0.249(1)
B	0.812(5)	0.232(4)	−0.154(2)	0.002(3)	−0.142(3)	−0.161(2)	−0.321(1)
C	1.175(6)	0.527(7)	0.059(4)	0.337(5)	0.014(5)	−0.037(3)	−0.241(1)
D	0.956(5)	0.582(6)	0.153(3)	0.320(5)	−0.015(4)	−0.062(2)	−0.173(1)
E	1.365(6)	1.020(8)	0.464(6)	1.040(8)	0.390(8)	0.278(4)	−0.018(1)
F	1.586(5)	1.404(8)	0.863(7)	1.280(8)	0.728(9)	0.618(6)	0.221(2)

small cross sections for direct photoionization. On the contrary, probabilities for population of satellite states by spectator RA decay transition are usually large.

Reference [56] suggests that the one-hole valence-ionized state $5a_1^{-1}$, produced by participator RA decay, contributes to the fifths and sixths energy intervals. Although, it has a noticeable direct photoionization cross section, population of this state via participator RA decay cannot explain the substantial signal observed in these binding energy intervals (see Fig. 2). We thus propose that the dominant signal observed in the fifth, sixth, and seventh intervals is due to intense spectator transitions populating final ionic states with two holes in different valence molecular orbitals (see the last column in Table II). The integral angular distribution parameters, representing the chosen binding energy intervals, are reported in Table III for different excitation energies. These quantities were determined from the angularly resolved spectra $\widetilde{I}_0$ and $\widetilde{I}_{90}$, integrated within the indicated energy intervals. The respective statistical uncertainties are listed in Table III in parentheses following each value of β. Those were estimated assuming a Poisson counting statistics for the integral photoelectron spectra $\widetilde{I}_0$ and $\widetilde{I}_{90}$. Thereafter, uncertainties in β parameters were calculated according to the procedure and formula from Ref. [57].

B. Participator RA decay

Before analyzing angular distributions of electrons released by the participator RA decay, we tested the quality of the electronic calculation in methyl chloride. For this purpose, we computed differential cross sections for the direct photoionization of the four outermost valence electrons, which correspond to the population of the $3e^{-1}(X\,^2E)$, $7a_1^{-1}(A\,^2A_1)$, $2e^{-1}(B\,^2E)$, and $6a_1^{-1}(C\,^2A_1)$ ionic states. The corresponding angular distribution parameters computed in a wide photoelectron energy range (not shown here) were found to be in very good agreement with the experimental β parameters reported in Ref. [56] for the first four binding energy intervals (see Fig. 3 in this reference).

Angular distribution parameters of RA electrons, computed for the participator X, A, B, and C final ionic states, are depicted in Fig. 4 by solid curves. These theoretical data are compared with the experimental angular distributions from Table III, which are determined at the selected photon energies for the first four binding energy intervals (indicated in each panel). Figure 4(a) illustrates the excellent agreement between the presently computed (solid curve) and measured β parameters for the $3e^{-1}(X\,^2E)$ final ionic state. For the $7a_1^{-1}(A\,^2A_1)$ state, good quantitative agreement between the computed and measured angular distribution parameters can be seen from Fig. 4(b). For the $2e^{-1}(B\,^2E)$ state, the experimental and theoretical β parameters in Fig. 4(c) exhibit an offset of about $\Delta\beta \approx 0.2$.

On the one hand, the disagreement between the theory and experiment seen from Figs. 4(b) and 4(c) can be related to the quality of the calculations, which decreases for higher excited states of the ion. On the other hand, the RA electron spectra of the $7a_1^{-1}(A\,^2A_1)$ and $2e^{-1}(B\,^2E)$ participator states strongly overlap: The corresponding bands in Fig. 2 form a broad hump, which spreads over both binding energy intervals. Therefore, a strict separation between these two participator states is not possible and their correspondence to intervals 2 and 3, suggested in Ref. [56], is only partial. The angular distribution parameter computed for the participator state $6a_1^{-1}(C\,^2A_1)$ differs substantially from the experimental values of β determined for the fourth binding energy interval of 20.8–22.9 eV [cf. solid curve and circles in Fig. 4(d)]. This large offset of about $\Delta\beta \approx 1.0$ between the computed and measured parameters will be discussed further in the next section.

From Fig. 4 one can see that the angular distribution parameters β, computed for the participator decay channels, exhibit strong energy dependences across the core-excited resonances of the molecule. This is a clear signature of the electronic-state interference, attributed to the presence of several ionization channels [15–19,23–26]. Far off-resonance, the computed β parameters follow trends imposed by the weak direct photoionization channel. Here angular emission distributions are characterized by the relatively large positive values of β. The angular distributions computed on resonance are determined by the dominant pathways for the excitation and RA decay of respective intermediate states and these β values are typically smaller. This causes broad dips in the computed angular distributions across the energy positions of the resonances.

The theoretical angular distribution parameters depicted in Fig. 4 by solid curves were computed utilizing the total transition amplitude (1), which implies a coherent superposition of the individual contributions of all ionization channels. In order to illustrate the pure effect of this interference, we performed

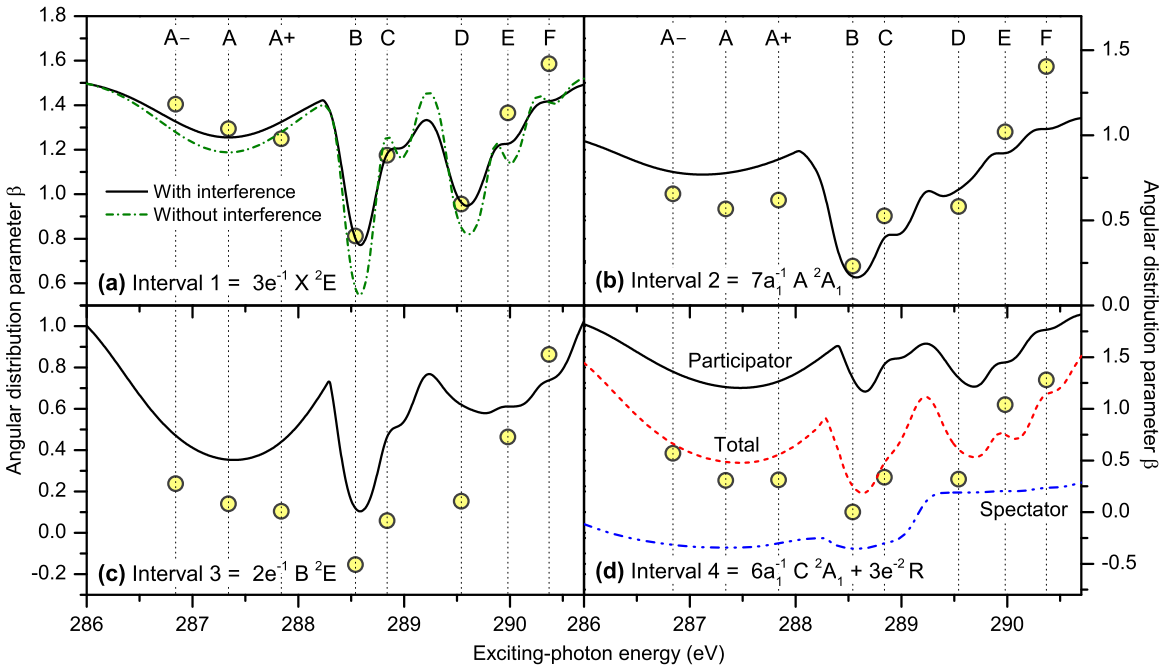

FIG. 4. Angular distribution parameters of RA electrons as functions of the photon energy, determined experimentally for different binding energy intervals and computed for selected participator and spectator RA decay channels (indicated in each panel). Experimental data shown by circles are the same as in Table III. Note also that experimental uncertainties (not shown) are smaller than the size of symbols. The selected excitation energies are indicated by the capital letters at the top and by the vertical dotted lines to guide the eye (see Table I for assignment). (a)–(c) Angular distribution parameters computed for respective participator transitions by including interference effects are shown by solid curves. In addition, the β parameter computed for the X state by neglecting interference effects is shown in (a) by a dash-dotted curve (see the text for more details). (d) Angular distributions computed for respective participator and spectator transitions are shown by solid and dash–double-dotted curves, whereas the total result is shown by the dashed curve. Note also the different vertical scales in each panel.

an additional calculation, in which individual contributions to the angular distribution parameters were taken incoherently. For this purpose, β parameters, computed separately for each channel, were weighted (averaged) with the respective cross sections. The result obtained for the $3e^{-1}(X\,^2E)$ final ionic state is illustrated in Fig. 4(a) by a dash-dotted curve. One can see that excluding interference effects substantially reduces the excellent agreement between the theory and experiment, which was achieved when this interference was included (cf. separately dash-dotted and solid curves with circles in the figure). Moreover, the interference makes dispersions of the computed angular distribution parameters across resonances somewhat broader.

C. Spectator RA decay

Accurate calculation of the RA electron spectra for spectator decay channels in methyl chloride is a formidable task. This is because, being coupled with different excited electrons, a large manifold of possible dicationic states with two holes in valence orbitals results in very rich multiplet structures of the final ionic states. In addition, a substantial contribution of shake-up (or shake-off) processes can be expected. Therefore, in the present work we made only an estimate of the angular distribution parameters of spectator RA electrons by a simplified theoretical model. In particular, we computed the normal Auger electron spectra of methyl chloride, assuming that the excited spectator electrons do not perturb very fast Auger electrons. Thereby, we considerably reduced the number of electronic states that need to be considered and described the whole multiplet structure of a final spectator state $a^{-1}b^{-1}R$ on average by a single angular distribution parameter (here a and b represent valence orbitals and R is the excited electron).

It is well known that the angular distribution of normal Auger electrons in molecules can be described by an inherent molecular frame angular distribution function, which is independent of the direction of polarization of exciting radiation [58–60]. Indeed, in the absence of postcollision interaction of photo- and Auger electrons, the angular emission correlation function between them can be factorized into two parts, one describing the photoionization step and the other Auger decay [61]. If photoelectrons are not observed in the experiment, one should integrate the former part over all photoelectron emission angles. This results in a prefactor determining the intensity of the Auger electron spectrum and its angular distribution is given solely by the second part. In the other words, how the core hole is created in the first step of the process is not relevant for Auger decay in the second step.

In the resonant Auger decay considered here, information on the light polarization remains imprinted in the excited electron however. In particular, depending on the symmetry of excitation, different molecular orientations will preferably contribute to the laboratory frame angular distribution after averaging over all possible orientations of a freely rotating molecule. In the case of methyl chloride, excitations of

TABLE IV. Angular distribution parameters estimated for different spectator RA transitions of the selected electronic resonances R. The theoretical values are averaged over the respective electronic multiplet structure of each final ionic state.

	$1s \rightarrow R$			
Final states	$8a_1$	$4sa_1$	$4pe$	$4pa_1$
$3e^{-2}R$	–0.38	–0.38	0.19	–0.38
$7a_1^{-1}3e^{-1}R$	0.32	0.32	–0.16	0.32
$2e^{-1}3e^{-1}R$	–0.38	–0.38	0.19	–0.38
$7a_1^{-2}R$	0.54	0.54	–0.27	0.54
$2e^{-1}7a_1^{-1}R$	0.32	0.32	–0.16	0.32
$2e^{-2}R$	–0.38	–0.38	0.19	–0.38

C $1s \rightarrow \mathrm{Ra}_1$ symmetry preselect molecules with the C-Cl molecular quantization axis oriented along the light's polarization direction and those of C $1s \rightarrow$ Re symmetry select alignment of the C-Cl axis perpendicular to the light's polarization. This can be seen in Table IV, where angular distribution parameters computed as discussed above for different $1s \rightarrow R$ initial excitations and some $a^{-1}b^{-1}R$ finals states of methyl chloride are collected. One can see that β parameters computed for the $1s \rightarrow 8a_1$, $4sa_1$, and $4pa_1$ excitations are equivalent (cf. the second, third, and fifth columns). Moreover, β parameters computed for the $1s \rightarrow 4pe$ excitation (fourth column) are related to the former parameters by $\beta_{\mathrm{Re}} = -\frac{1}{2}\beta_{\mathrm{Ra}_1}$. This is a direct consequence of the selection of the two mutually orthogonal molecular orientations in the excitation step depending upon the symmetry of the excited state. Finally, β parameters obtained within our simplified theoretical model for a particular combination of symmetries of the a^{-1} and b^{-1} valence orbitals are equal (cf. the data listed in the first, third, and last rows of the table for the $e^{-1}e^{-1}$ combination and separately data listed in the second and fifth rows for the $e^{-1}a_1^{-1}$ combination).

Let us now analyze the obtained theoretical results in more detail. From Fig. 4(d) it is evident that the theoretical angular distribution parameter, computed for the participator transition populating the $6a_1^{-1}(C\,^2A_1)$ state, does not reproduce the experimental observations for the fourth binding energy interval of 20.8–22.9 eV. This is because the $3e^{-2}R$ final ionic states, populated via spectator RA decay, fall in this binding energy interval as well. An averaged β parameter computed for these spectator transitions is depicted in Fig. 4(d) by a dash–double-dotted curve. This result was obtained by incoherent overlap of the individual contributions listed in the first row of Table IV, since different $1s \rightarrow R$ resonances populate different final ionic states $3e^{-2}R$. According to this table, it changes sign in between resonances C and D. The total angular distribution parameter, averaged over the two contributions from the participator and spectator RA decay transitions, is depicted in Fig. 4(d) by a dashed curve. One can see that including contributions from the $3e^{-2}R$ spectator state brings the theoretical β parameter into good agreement with the experimental values.

The other spectator states considered theoretically, listed in the second to sixth rows of Table IV, have binding energies larger than those of the $3e^{-2}R$ states and they contribute to the energy intervals 5–7 (see also assignment in Table II). It is difficult to perform a more accurate assignment, since each electronic multiplet $a^{-1}b^{-1}R$ is typically spread over a 1–2 eV energy range and its central binding energy depends on the excited electron R. Nuclear motion introduces additional broadening to each electronic line. As a consequence, individual spectra of the spectator transitions listed in Table IV strongly overlap. Therefore, it is not straightforward to compare the theoretical angular distribution parameters from Table IV with the experimental β parameters for the binding energy intervals 5–7 (last three columns of Table III). Nevertheless, an indirect comparison between the present theory and experiment is still possible.

For this purpose, we notice that the theoretical β parameters listed in Table IV are relatively small. Moreover, the sum of β parameters computed for each resonance (in each column of the table) is very close to zero. Therefore, the average angular distribution for all unresolved spectator RA electrons is almost isotropic at each excitation energy. This is a rather general situation, which can be illustrated with the example of closed-shell atoms. For instance, angular distribution parameters for the K-$L_1L_{2,3}$ spectator RA decay channels of Ne $1s^12s^22p^6np\,^1P \rightarrow 1s^22s^12p^5(^1P,^3P)np\,^2S,^2P,^2D + \varepsilon\ell$ are equal to $\beta_{^2S} = 2$, $\beta_{^2P} = -1$, and $\beta_{^2D} = 0.2$. Averaging these partial contributions with the respective intensities (scale statistically as 1:3:5 for the S, P, and D states, respectively), one obtains that the angular distribution parameter for the whole K-$L_1L_{2,3}$ spectator RA transition in Ne is equal to zero.

The present experimental results confirm this general trend for spectator RA electrons of methyl chloride. As one can see from Table IV, β parameters measured for the 5–7 binding energy intervals are rather small, except the two values obtained for the F resonance (last row) in the fifth and sixth intervals. The latter deviations can be rationalized as follows. The angular distribution parameter computed for the direct ionization of the $5a_1^{-1}$ ionic state (which also falls in these binding energy intervals; see Table II) is equal to $\beta \approx 2$ and at higher excitation energies its contribution starts to dominate over contributions from the resonant channels.

V. CONCLUSION

The excitation and resonant Auger decay of methyl chloride is studied below the C 1s ionization threshold. Experimentally, RA electron spectra, induced by excitation with linearly polarized synchrotron radiation at photon energies corresponding to the $1s \rightarrow 8a_1$, $4sa_1$, $4pe$, and $4pa_1$ excitations of carbon, are recorded with angular resolution over the wide interval of binding energies of 11–37 eV. This allowed determination of the vibrationally unresolved angular distribution parameters for several selected binding energy intervals, encompassing either a single well-separated state or a few overlapping final electronic states of the CH_3Cl^+ ion. Theoretically, electronic amplitudes for the resonant Auger transition in the CH_3Cl molecule are calculated by the single-center method in the relaxed-core Hartree-Fock approximation. The accompanying nuclear dynamics is simulated using a one-dimensional model describing dissociation of the C $1s \rightarrow 8a_1$ state along the C-Cl

coordinate, as well as the symmetric CH stretching in the considered C $1s \rightarrow 4\ell$ core-excited Rydberg states.

The theoretical angular distribution parameters of RA electrons, computed for the participator transitions populating the X, A, and B electronic states of CH_3Cl^+, are in good agreement with the experimental values of the integral β parameters, determined for the first three binding energy intervals encompassing these states. In particular, the measured β parameters exhibit strong variations with the excitation energy across the electronic resonances. This is due to an interplay between the direct and the resonant ionization pathways. The consideration of electronic-state interference in the calculation of the transition amplitudes towards participator final states improves the agreement between the computed and the measured β parameters. The present calculations suggest that the fourth binding energy interval of 20.8–22.9 eV contains RA electrons from the participator transition populating the C electronic state of the ion, as well as from the spectator transitions populating final ionic states with two holes in the highest occupied molecular orbital. Furthermore, we assign intervals with higher binding energies to spectator transitions populating electronic states with the two holes in other valence orbitals. Here, after averaging over the manifold of overlapping final ionic states, one expects an almost isotropic emission distribution with small values of β. This trend is confirmed by the present observations.

Our study paves the way for future investigations of ESI in the RA decay of methyl chloride. For this purpose, several approximations in the present theory (e.g., the one-particle Hartree-Fock approximation for the photoelectron in continuum, the fixed nuclei approximation for calculations of the electron transition matrix elements, and the one-dimensional simulations of the nuclear dynamics) need to be lifted. From the experimental point of view, measuring β parameters at additional on- and off-resonance photon energies below the K edge of carbon atom could provide deeper insight into our understanding of the effect.

ACKNOWLEDGMENTS

We thank E. Robert for technical assistance and the SOLEIL staff for the stable operation of the equipment and the storage ring during the experiments (Proposal No. 20151032). S.N. would like to acknowledge fruitful discussions with M. Patanen during the initial stage of the data analysis. We also thank I. D. Petrov for many valuable discussions. Financial support from the Deutsche Forschungsgemeinschaft (Project No. DE 2366/1-1) and the Russian Foundation for Basic Research (Grant No. 16-03-00771a) is gratefully acknowledged. P.V.D. acknowledges Research Institute of Physics, Southern Federal University for the hospitality during his research stay there.

[1] A. Cesar and H. Ågren, Phys. Rev. A **45**, 2833 (1992).
[2] N. M. Kabachnik, S. Fritzsche, A. N. Grum-Grzhimailo, M. Meyer, and K. Ueda, Phys. Rep. **451**, 155 (2007).
[3] G. B. Armen, J. C. Levin, and I. A. Sellin, Phys. Rev. A **53**, 772 (1996).
[4] J.-E. Rubensson, M. Neeb, A. Bringer, M. Biermann, and W. Eberhardt, Chem. Phys. Lett. **257**, 447 (1996).
[5] E. Kukk, H. Aksela, A. Kivimaäki, J. Jauhiainen, E. Nõmmiste, and S. Aksela, Phys. Rev. A **56**, 1481 (1997).
[6] T. LeBrun, S. H. Southworth, G. B. Armen, M. A. MacDonald, and Y. Azuma, Phys. Rev. A **60**, 4667 (1999).
[7] N. Saito, N. M. Kabachnik, Y. Shimizu, H. Yoshida, H. Ohashi, Y. Tamenori, I. H. Suzuki, and K. Ueda, J. Phys. B **33**, L729 (2000).
[8] B. M. Lagutin, Ph. V. Demekhin, V. L. Sukhorukov, A. Ehresmann, and H. Schmoranzer, J. Phys. B **36**, L163 (2003).
[9] R. K. Kushawaha, K. Jänkälä, T. Marchenko, G. Goldsztejn, R. Guillemin, L. Journel, D. Céolin, J.-P. Rueff, A. F. Lago, R. Püttner, M. N. Piancastelli, and M. Simon, Phys. Rev. A **92**, 013427 (2015).
[10] G. Goldsztejn, R. Püttner, L. Journel, R. Guillemin, O. Travnikova, R. K. Kushawaha, B. Cunha de Miranda, I. Ismail, D. Céolin, M. N. Piancastelli, M. Simon, and T. Marchenko, Phys. Rev. A **95**, 012509 (2017).
[11] G. Goldsztejn, T. Marchenko, D. Céolin, Loïc Journel, R. Guillemin, J.-P. Rueff, R. K. Kushawaha, R. Püttner, M. N. Piancastelli, and M. Simon, Phys. Chem. Chem. Phys. **18**, 15133 (2016).
[12] V. Schmidt, Rep. Prog. Phys. **55**, 1483 (1992).
[13] C. Miron and P. Morin, in *Handbook of High-Resolution Spectroscopy*, edited by M. Quack and F. Merkt (Wiley, Chichester, 2011).
[14] F. K. Gel'mukhanov, L. N. Mazalov, and A. V. Kondratenko, Chem. Phys. Lett. **46**, 133 (1977).
[15] B. M. Lagutin, I. D. Petrov, V. L. Sukhorukov, S. Kammer, S. Mickat, R. Schill, K.-H. Schartner, A. Ehresmann, Y. A. Shutov, and H. Schmoranzer, Phys. Rev. Lett. **90**, 073001 (2003).
[16] B. M. Lagutin, I. D. Petrov, V. L. Sukhorukov, Ph. V. Demekhin, B. Zimmermann, S. Mickat, S. Kammer, K.-H. Schartner, A. Ehresmann, Y. A. Shutov, and H. Schmoranzer, J. Phys. B **36**, 3251 (2003).
[17] K.-H. Schartner, R. H. Schill, D. Hasselkamp, S. Mickat, S. Kammer, L. Werner, S. Klumpp, A. Ehresmann, H. Schmoranzer, B. M. Lagutin, and V. L. Sukhorukov, J. Phys. B **38**, 4155 (2005).
[18] K.-H. Schartner, R. Schill, D. Hasselkamp, S. Mickat, S. Kammer, L. Werner, S. Klumpp, A. Ehresmann, H. Schmoranzer, B. M. Lagutin, and V. L. Sukhorukov, J. Phys. B **40**, 1443 (2007).
[19] S. Heinasmäki, K. Jänkälä, and J. Niskanen, J. Phys. B **42**, 085002 (2009).
[20] E. Kukk, J. D. Bozek, W.-T. Cheng, R. F. Fink, A. A. Wills, and N. Berrah, J. Chem. Phys. **111**, 9642 (1999).
[21] O. Hemmers, F. Heiser, J. Viefhaus, K. Wieliczek, and U. Becker, J. Phys. B **32**, 3769 (1999).
[22] H. Wang, R. F. Fink, M. N. Piancastelli, M. Bässler, I. Hjelte, O. Björneholm, F. Burmeister, R. Feifel, A. Giertz, C. Miron, S. L. Sorensen, K. Wiesner, and S. Svensson, Chem. Phys. **289**, 31 (2003).

[23] P. V. Demekhin, I. D. Petrov, V. L. Sukhorukov, W. Kielich, P. Reiss, R. Hentges, I. Haar, H. Schmoranzer, and A. Ehresmann, Phys. Rev. A **80**, 063425 (2009); **81**, 069902(E) (2010).
[24] P. V. Demekhin, I. D. Petrov, T. Tanaka, M. Hoshino, H. Tanaka, K. Ueda, W. Kielich, and A. Ehresmann, J. Phys. B **43**, 065102 (2010).
[25] P. V. Demekhin, I. D. Petrov, V. L. Sukhorukov, W. Kielich, A. Knie, H. Schmoranzer, and A. Ehresmann, Phys. Rev. Lett. **104**, 243001 (2010).
[26] P. V. Demekhin, I. D. Petrov, V. L. Sukhorukov, W. Kielich, A. Knie, H. Schmoranzer, and A. Ehresmann, J. Phys. B **43**, 165103 (2010).
[27] A. Lindblad, V. Kimberg, J. Söderström, C. Nicolas, O. Travnikova, N. Kosugi, F. Gel'mukhanov, and C. Miron, New J. Phys. **14**, 113018 (2012).
[28] C. Miron, V. Kimberg, P. Morin, C. Nicolas, N. Kosugi, S. Gavrilyuk, and F. Gel'mukhanov, Phys. Rev. Lett. **105**, 093002 (2010).
[29] Y. Shimizu, H. Ohashi, Y. Tamenori, Y. Muramatsu, H. Yoshida, K. Okada, N. Saito, H. Tanaka, I. Koyano, S. Shin, and K. Ueda, J. Electron Spectrosc. Relat. Phenom. **114–116**, 63 (2001).
[30] I. Hjelte, L. Karlsson, S. Svensson, A. De Fanis, V. Carravetta, N. Saito, M. Kitajima, H. Tanaka, H. Yoshida, A. Hiraya, I. Koyano, K. Ueda, and M. N. Piancastelli, J. Chem. Phys. **122**, 084306 (2005).
[31] A. Knie, M. Ilchen, P. Schmidt, P. Reiß, C. Ozga, B. Kambs, A. Hans, N. Müglich, S. A. Galitskiy, L. Glaser, P. Walter, J. Viefhaus, A. Ehresmann, and P. V. Demekhin, Phys. Rev. A **90**, 013416 (2014).
[32] E. Antonsson, M. Patanen, C. Nicolas, S. Benkoula, J. J. Neville, V. L. Sukhorukov, J. D. Bozek, P. V. Demekhin, and C. Miron, Phys. Rev. A **92**, 042506 (2015).
[33] A. Knie, M. Patanen, A. Hans, I. D. Petrov, J. D. Bozek, A. Ehresmann, and P. V. Demekhin, Phys. Rev. Lett. **116**, 193002 (2016).
[34] A. P. Hitchcock and C. E. Brion, J. Electron Spectrosc. Relat. Phenom. **13**, 193 (1978).
[35] A. P. Hitchcock and C. E. Brion, J. Electron Spectrosc. Relat. Phenom. **14**, 417 (1978).
[36] D. Céolin, M. N. Piancastelli, R. Guillemin, W. C. Stolte, S.-W. Yu, O. Hemmers, and D. W. Lindle, J. Chem. Phys. **126**, 084309 (2007).
[37] M. N. Piancastelli, G. Goldsztejn, T. Marchenko, R. Guillemin, R. K. Kushawaha, L. Journel, S. Carniato, J.-P. Rueff, D. Céolin, and M. Simon, J. Phys. B **47**, 124031 (2014).
[38] C. Miron, P. Morin, D. Céolin, L. Journel, and M. Simon, J. Chem. Phys. **128**, 154314 (2008).
[39] T. Marchenko, L. Journel, T. Marin, R. Guillemin, S. Carniato, M. Žitnik, M. Kavčič, K. Bučar, A. Mihelič, J. Hoszowska, W. Cao, and M. Simon, J. Chem. Phys. **134**, 144308 (2011).
[40] J. Söderström, A. Lindblad, A. Grum-Grzhimailo, O. Travnikova, N. Nicolas, S. Svensson, and C. Miron, New J. Phys. **13**, 073014 (2011).
[41] O. Travnikova, J. C. Liu, A. Lindblad, C. Nicolas, J. Söderström, V. Kimberg, F. Gel'mukhanov, and C. Miron, Phys. Rev. Lett. **105**, 233001 (2010).
[42] M. Patanen, C. Nicolas, X.-J. Liu, O. Travnikova, and C. Miron, Phys. Chem. Chem. Phys. **15**, 10112 (2013).
[43] O. Sublemontier, C. Nicolas, D. Aureau, M. Patanen, H. Kintz, X. Liu, M.-A. Gaveau, J.-L. Le Garrec, E. Robert, F.-A. Barreda, A. Etcheberry, C. Reynaud, J. B. Mitchell, and C. Miron, J. Phys. Chem. Lett. **5**, 3399 (2014).
[44] A. R. Milosavljević, F. Canon, C. Nicolas, C. Miron, L. Nahon, and A. Giuliani, J. Phys. Chem. Lett. **3**, 1191 (2012).
[45] M. Ilchen, G. Hartmann, P. Rupprecht, A. N. Artemyev, R. N. Coffee, Z. Li, H. Ohldag, H. Ogasawara, T. Osipov, D. Ray, P. Schmidt, T. J. A. Wolf, A. Ehresmann, S. Moeller, A. Knie, and P. V. Demekhin, Phys. Rev. A **95**, 053423 (2017).
[46] M. Tia *et al.*, J. Phys. Chem. Lett. **8**, 2780 (2017).
[47] P. V. Demekhin, A. Ehresmann, and V. L. Sukhorukov, J. Chem. Phys. **134**, 024113 (2011).
[48] S. A. Galitskiy, A. N. Artemyev, K. Jänkälä, B. M. Lagutin, and P. V. Demekhin, J. Chem. Phys. **142**, 034306 (2015).
[49] A. N. Artemyev, A. D. Müller, D. Hochstuhl, and P. V. Demekhin, J. Chem. Phys. **142**, 244105 (2015).
[50] A. Ehresmann, L. Werner, S. Klumpp, H. Schmoranzer, P. V. Demekhin, B. M. Lagutin, V. L. Sukhorukov, S. Mickat, S. Kammer, B. Zimmermann, and K. H. Schartner, J. Phys. B **37**, 4405 (2004).
[51] P. V. Demekhin, D. V. Omel'yanenko, B. M. Lagutin, V. L. Sukhorukov, L. Werner, A. Ehresmann, K.-H. Schartner, and H. Schmoranzer, Opt. Spektrosc. **102**, 318 (2007).
[52] A. Ehresmann, P. V. Demekhin, W. Kielich, I. Haar, M. A. Schlüter, V. L. Sukhorukov, and H. Schmoranzer, J. Phys. B **42**, 165103 (2009).
[53] P. V. Demekhin, V. L. Sukhorukov, H. Schmoranzer, and A. Ehresmann, J. Chem. Phys. **132**, 204303 (2010).
[54] P. Piecuch, S. A. Kucharski, K. Kowalski, and M. Musial, Comput. Phys. Commun. **149**, 71 (2002).
[55] H.-J. Werner, P. J. Knowles, G. Knizia, F. R. Manby, and M. Schütz, Comput. Mol. Sci. **2**, 242 (2012).
[56] D. M. P. Holland, I. Powis, G. Öhrwall, L. Karlsson, and W. von Niessen, Chem. Phys. **326**, 535 (2006).
[57] M. Patanen, O. Travnikova, M. G. Zahl, J. Söderström, P. Decleva, T. D. Thomas, S. Svensson, N. Mårtensson, K. J. Børve, L. J. Sæthre, and C. Miron, Phys. Rev. A **87**, 063420 (2013).
[58] T. Jahnke, A. Czasch, M. Schöffler, S. Schössler, M. Käsz, J. Titze, K. Kreidi, R. E. Grisenti, A. Staudte, O. Jagutzki, L. P. H. Schmidt, S. K. Semenov, N. A. Cherepkov, H. Schmidt-Böcking, and R. Dörner, J. Phys. B **40**, 2597 (2007).
[59] K. Kreidi *et al.*, J. Phys. B **41**, 101002 (2008).
[60] S. K. Semenov *et al.*, Phys. Rev. A **85**, 043421 (2012).
[61] V. V. Kuznetsov and N. A. Cherepkov, J. Electron Spectrosc. Relat. Phenom. **79**, 437 (1996).